

Title: A New Framework for Nonlinear Kalman Filters

Authors:

Shida Jiang,^{1*} Junzhe Shi,¹ Scott Moura¹

Affiliations:

¹Department of Civil and Environmental Engineering, University of California, Berkeley, Berkeley, CA, USA.

*Corresponding author. Email: shida_jiang@berkeley.edu.

Abstract: The Kalman filter (KF) is a state estimation algorithm that optimally combines system knowledge and measurements to minimize the mean squared error of the estimated states. While KF was initially designed for linear systems, numerous extensions of it, such as extended Kalman filter (EKF), unscented Kalman filter (UKF), cubature Kalman filter (CKF), etc., have been proposed for nonlinear systems. Although different types of nonlinear KFs have different pros and cons, they all use the same framework of linear KF. Yet, according to what we found in this paper, the framework tends to give overconfident and less accurate state estimations when the measurement functions are nonlinear. Therefore, in this study, we designed a new framework for nonlinear KFs and showed theoretically and empirically that the new framework estimates the states and covariance matrix more accurately than the old one. The new framework was tested on four different nonlinear KFs and five different tasks, showcasing its ability to reduce the estimation errors by several orders of magnitude in low-measurement-noise conditions, with only about a 10–90% increase in computational time. All types of nonlinear KFs can benefit from the new framework, and the benefit will increase as the sensors become more and more accurate in the future. As an example, EKF, the simplest nonlinear KF that was previously believed to work poorly for strongly nonlinear systems, can now provide fast and fairly accurate state estimations with the help of the proposed new framework. The codes are available at [this URL](#).

One-Sentence Summary: This paper presents a new framework that significantly improves the performance of all types of nonlinear Kalman filters.

Main Text:

INTRODUCTION

In control theory, the KF is a state estimation algorithm designed for linear systems. In such a system, a set of linear state transition functions describes how the states evolve, and a set of linear measurement functions describes the measured values of certain linear combinations of states. It is assumed that both the state transition and measurement functions contain some additive noise. The KF optimally combines the system knowledge and measurements to minimize the sum of the states' variances when both process and measurement noise follow a normal (Gaussian) distribution. Since its birth in about 1960, KF has achieved massive success in navigation (1), motion control (2), statistics (3), signal processing (4), etc.

The most significant limitation of KF is that it can only be applied to systems with linear state transition functions and linear measurement functions. Unfortunately, many real-life systems are nonlinear (5). Therefore, some extensions of KF have been developed to solve the state estimation problem for these nonlinear systems, and the most well-known ones are EKF and UKF.

EKF linearizes the state transition functions and measurement functions locally at each time step (5). This technique transforms the nonlinear system into a linear system, where KF can be directly applied. While EKF is relatively simple, the linearization performed in each step neglects the higher-order derivatives, making the state estimations biased and overconfident. Specifically, estimations can be biased since $\mathbb{E}(f(x)) = f(\mathbb{E}(x))$ is not guaranteed for a nonlinear function f , and overconfidence arises when the actual variance is much higher than estimated. These problems are partially solved by the second-order extended Kalman filter (EKF2) (6), which approximates the nonlinear system by its second-order Taylor expansion. However, EKF2 requires the calculation of the Hessian matrix of each state transition function and measurement function, which adds non-trivial computational complexity to the algorithm. Additionally, EKF2 still sometimes gives inaccurate and overconfident estimations, so it is generally used less frequently than EKF.

Both EKF and EKF2 require the calculation of the Jacobian matrices of the state transition functions and measurement functions, which may not always be accessible in real-life systems. In 1997, Simon et al. introduced another extension of KF to nonlinear systems that requires no direct calculation of the Jacobian matrix and avoids the accuracy loss caused by linearization (7). In later literature, this extension is usually referred to as the UKF (8). UKF approximates the distribution of the states after nonlinear transformations by sampling several points (called sigma points) around the estimated mean of the states. These points go through the same transformation as the mean, and a more accurate estimation of the states' distribution after the transformation can be obtained with the help of these extra sample points. In UKF, the sigma points are selected deterministically based on each state's standard deviation. This technique guarantees that the sigma points are evenly distributed around the central point and can provide a more accurate state estimation. Similar ideas have also been used in several other nonlinear KFs, including cubature Kalman filter (CKF) (9), quadrature Kalman filter (10), square-root quadrature Kalman filter (11), etc. All these filters use deterministic ways to find several additional points around the central point (the estimated states from the previous iteration) and use those points to approximate the first two moments of the states after the nonlinear transformation. All these methods have some links with EKF2. As pointed out by Gustafsson et al. in (12), when the sigma points are infinitely close to the center, and the hyperparameters in the UKF are set to specific values, UKF will give the exact estimation as the EKF2. A disadvantage of these nonlinear KFs is that the number of sampling points is at least twice the number of states. Therefore, the method can be increasingly more complicated than EKF as the number of states increases.

While different extensions of the KF use various ways to approximate the first two moments of the states after a nonlinear transformation, they all follow the same framework as in the linear KF. In such a framework, the state estimations in each iteration can be divided into two steps: Predict and Update. In the "Predict" step, the state and covariance estimations are predicted using the state transition function and estimates from the previous iteration. Then, in the "Update" step, the measurements correct the state predictions with a feedback gain (also known as the Kalman gain), which is designed to minimize the trace of the states' covariance matrix after the update. After the states are updated, the state covariance matrix is also updated, ending the present iteration. Note that the covariance matrix will have the smallest possible trace after the update since that's how the Kalman gain is selected.

However, there is a problem with this final step in the iteration. As shown in the example in Fig. 1, calculating the Kalman gain requires approximating the nonlinear measurement functions around the predicted states, either explicitly as in EKF or implicitly as in UKF. After the update, however, such an approximation may no longer be accurate because the predicted states can be far away from the updated states, as suggested by the difference between the purple dashed lines Approx. 1 and 2 in Fig. 1. Therefore, the Kalman gain, which was optimized based on the approximated measurement function near the predicted states, will not, in general, minimize the trace of the covariance matrix after the update. This is because the states will move to a new location after the update, and the previous approximations may be inaccurate. Since the conventional framework for nonlinear KFs assumes that the Kalman gain is optimal, it often underestimates the trace of the covariance matrix. For example, in Fig. 1, the actual state estimation error $|x_{k|k} - x_k|$ becomes greater than the estimated standard deviation $\sigma_{k|k}$ after the state update because the effectiveness of the Kalman gain is overestimated. This is visualized by the narrow yellow distribution in Step 2: Update, which does not cover the true state. In other words, the conventional framework inherently tends to give overconfident covariance estimation when the measurement functions are nonlinear.

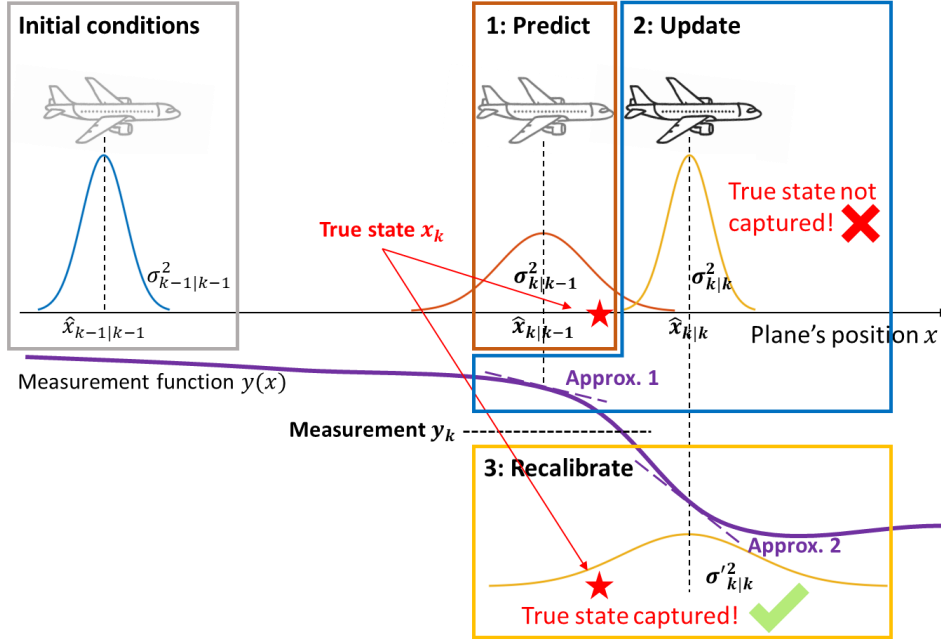


Fig. 1. The basic idea of the new framework of nonlinear Kalman filter. The conventional framework only uses the first two steps and approximates the measurement functions around the predicted states. The additional step we propose recalculates the approximation of the nonlinear measurement function around the updated states, making the final covariance estimation more accurate. The example shown here illustrates an extended Kalman filter for terrain-referenced navigation. The measurement function is the altitude of the ground beneath the plane, which is a nonlinear function of the plane's position.

The problem described above will become increasingly significant as the measurement noise decreases, and the measurements play a more critical role in the state estimation. In some circumstances, it can even lead to a highly undesirable and counterintuitive phenomenon: the actual estimation error increases as the measurement noise decreases. The primary cause of this phenomenon is that the actual estimation errors drop much slower than the estimated standard deviations, and such overconfidence prevents the filter from correcting itself in later iterations. As the development of technology makes all types

of sensors more and more accurate, we can reasonably predict that this problem will become increasingly severe if we stick to the conventional framework for nonlinear KFs.

Once we fundamentally understand this problem, the solution is simple. We can redo the approximation after the update and use the newly approximated measurement function to update the covariance estimation. In our new framework, this new step is called “recalibrate”. As shown in Fig. 1, with this additional step, the covariance matrix may not have the smallest possible trace after the update; instead, it will honestly reflect the effect of the Kalman gain on the state covariance matrix. This is visualized by the wider yellow distribution in Step 3: Recalibrate which now covers the true state.

It is worth mentioning that when the measurement functions are all linear, they would require no approximation. Or, to be more precise, the approximation of the measurement functions would become independent of the states. In this case, the covariance estimation will not change before and after the recalibration, and our framework will be equivalent to the conventional framework.

The new framework described above may remind the readers of the iterated Kalman filter (IKF), which also re-approximates the measurement function after calculating the Kalman gain (13–15). However, IKF is fundamentally different from our framework in three ways. Firstly, IKF redoes the approximation and recalculates the Kalman gain iteratively until convergence. However, such a convergence is not guaranteed, so the algorithm is less robust and often requires finetuning the step size of each iteration (16). Even if the iteration converges, the convergence may take a very long time. By contrast, the new framework requires no iteration, and the re-approximation is only done once. Secondly, IKF was initially only used on EKF, and the deduction of iterated EKF (IEKF) requires an explicit approximation of the measurement function, which is only possible for EKF and EKF2. Although a few attempts have been made to extend IKF to UKF and CKF (14, 15, 17, 18), a consensus on how to do this robustly has not been reached. Therefore, it is not easy to implement IKF on all types of nonlinear KFs while guaranteeing that the estimator can converge in most cases. Our framework, on the other hand, does not have this problem since there is no convergence issue. Thirdly, and most importantly, the basic idea behind IKF is still to find the optimal Kalman gain and not to accurately estimate the covariance matrix. Indeed, these two objectives can be achieved simultaneously when the Kalman gain of IKF converges. Yet, when it fails to converge (which actually happens quite often in practice), IKF will still update the states and covariance matrix simultaneously, resulting in overconfident state estimations. In general, in terms of making a more accurate estimation, finding the optimal Kalman gain is not as important as making the covariance estimation accurate, as we will discuss later in the simulation results.

RESULTS

The new framework for nonlinear Kalman filters

Consider a system with the following dynamics:

$$x_k = f(x_{k-1}, u_{k-1}) + w_{k-1} \quad (1)$$

where x_k are the true states at the time step k , u_k are the inputs at the time step k , and w_k are the process noises that follow the zero-mean multivariate Gaussian distribution with covariance Q_k . The estimations of the states made in the previous step are denoted as $\hat{x}_{k-1|k-1}$. Since the true states are unknown, the KF assumes that the estimation errors $\hat{x}_{k-1|k-1} - x_{k-1}$ follow the zero-mean multivariate Gaussian distribution with covariance $P_{k-1|k-1}$. Whichever nonlinear KF is used, the first step of each iteration is called “Predict”, which predicts the states using (Eq. 1) and the estimations made in the previous time step. The predicted states are denoted as $\hat{x}_{k|k-1}$, and the errors $\hat{x}_{k|k-1} - x_k$ are assumed to follow the zero-mean multivariate Gaussian distribution with covariance $P_{k|k-1}$.

The second step of each iteration for any nonlinear KF is called “Update”, which corrects the predicted states based on the measurements. Suppose that the measurements of the states are as follows:

$$z_k = h(x_k) + v_k \quad (2)$$

where z_k are the measurements at the time step k , and v_k are the measurement noises that follow the zero-mean multivariate Gaussian distribution with covariance R_k . Given (Eq. 2) and the predicted states, the measurements can also be predicted using a particular method specific to the type of nonlinear KF. The predicted measurements are denoted as $\hat{y}_{k|k-1}$, whose errors $\hat{y}_{k|k-1} - h(x_k)$ are assumed to follow the zero-mean multivariate Gaussian distribution with covariance $P_{y,k|k-1}$. The cross-covariance matrix between the predicted states and the predicted measurements is denoted as $P_{xy,k|k-1}$. The differences between the predicted and actual measurements are called the measurement residuals $\tilde{y}_k = z_k - \hat{y}_{k|k-1}$. If we assume that the measurement noises are independent from the predicted states, then \tilde{y}_k should have zero mean, and their covariance $S_{k|k-1}$ can be calculated by:

$$S_{k|k-1} = P_{y,k|k-1} + R_k \quad (3)$$

KFs use the following equation to update the state estimation:

$$\hat{x}_{k|k} = \hat{x}_{k|k-1} + K_k \tilde{y}_k \quad (4)$$

where $\hat{x}_{k|k}$ are the updated states, and K_k is the Kalman gain. With (Eq. 3, 4), the covariance of $\hat{x}_{k|k}$ can be calculated as:

$$P_{k|k} = P_{k|k-1} + K S_{k|k-1} K^T - P_{xy,k|k-1} K^T - K P_{xy,k|k-1}^T \quad (5)$$

KFs select the Kalman gain to minimize the trace of $P_{x,k|k}$. By taking the derivative of (Eq. 5), we notice that the trace is minimized when:

$$K_k = P_{xy,k|k-1} S_{k|k-1}^{-1} \quad (6)$$

In this case, (Eq. 5) becomes:

$$P_{k|k} = P_{k|k-1} - K S_{k|k-1} K^T \quad (7)$$

(Eq. 4) and (Eq. 7) are the final two equations used in each iteration of the conventional framework of nonlinear KFs. However, as we mentioned in the Introduction, all the covariance matrices in (Eq. 5) are estimated based on the predicted states. Therefore, after the states are updated using (Eq. 4), P_{xy}, P_y, S should also be updated before the state covariance matrix is updated. This step is called “recalibrate” and is the key contribution of this manuscript. Namely, P_{xy}, P_y, S are all re-estimated based on $\hat{x}_{k|k}$. Then, $P_{k|k}$ is estimated as follows:

$$P_{k|k} = P_{k|k-1} + K S_{k|k} K^T - P_{xy,k|k} K^T - K P_{xy,k|k}^T \quad (8)$$

The difference between (Eq. 8) and (Eq. 7) highlights the fundamental idea of the new framework. That is, instead of reducing the updated state covariance matrix to the smallest possible value, we re-approximate the system after the state update to estimate the actual effect of the Kalman gain more accurately. In fact, in the new framework, the trace of the covariance matrix may increase after the recalibration if the system is strongly nonlinear and the predicted states have large variances, just like the example shown in Fig. 1. This phenomenon means that the update fails to make the estimation more accurate and should be withdrawn. To address this situation, we also add a “back out” step to the framework, which allows the state estimator to back out of the update when the update is unhelpful. The pseudo-code of the new framework is shown in Fig. 2.

Input: Process noise covariance matrix \mathbf{Q}_k , Measurement noise covariance matrix \mathbf{R}_k , state transition function $\mathbf{f}(\mathbf{x}, \mathbf{u})$, measurement function $\mathbf{h}(\mathbf{x})$, system inputs \mathbf{u}_k , measurements \mathbf{z}_k

Initialization:

- 1: $\hat{\mathbf{x}}_{0|0} = \mathbb{E}[\mathbf{x}_0]$
- 2: $\mathbf{P}_{0|0} = \mathbb{E}[(\hat{\mathbf{x}}_{0|0} - \mathbf{x}_0)(\hat{\mathbf{x}}_{0|0} - \mathbf{x}_0)^T]$
- 3: **for** every time step k **do**
- Predict:**
- 4: Estimate $\hat{\mathbf{x}}_{k|k-1}$ and $\mathbf{P}_{k|k-1}$ based on $\hat{\mathbf{x}}_{k-1|k-1}$, $\mathbf{P}_{k-1|k-1}$, \mathbf{f} , \mathbf{u}_k , and \mathbf{Q}_k
- Update:**
- 5: Estimate $\hat{\mathbf{y}}_{k|k-1}$, $\mathbf{P}_{xy,k|k-1}$ and $\mathbf{P}_{y,k|k-1}$ based on $\hat{\mathbf{x}}_{k|k-1}$, $\mathbf{P}_{k|k-1}$, and \mathbf{h}
- 6: $\mathbf{S}_{k|k-1} = \mathbf{P}_{y,k|k-1} + \mathbf{R}_k$
- 7: $\mathbf{K} = \mathbf{P}_{xy,k|k-1} \mathbf{S}_{k|k-1}^{-1}$
- 8: $\hat{\mathbf{x}}_{k|k} = \hat{\mathbf{x}}_{k|k-1} + \mathbf{K}(\mathbf{z}_k - \hat{\mathbf{y}}_{k|k-1})$
- Recalibration:**
- 9: Estimate $\mathbf{P}_{xy,k|k}$ and $\mathbf{P}_{y,k|k}$ based on $\hat{\mathbf{x}}_{k|k}$, $\mathbf{P}_{k|k-1}$, and \mathbf{h}
- 10: $\mathbf{S}_{k|k} = \mathbf{P}_{y,k|k} + \mathbf{R}_k$
- 11: $\mathbf{P}_{k|k} = \mathbf{P}_{k|k-1} + \mathbf{K} \mathbf{S}_{k|k} \mathbf{K}^T - \mathbf{P}_{xy,k|k} \mathbf{K}^T - \mathbf{K} \mathbf{P}_{xy,k|k}^T$
- Back out:**
- 12: **if** $\text{tr}(\mathbf{P}_{k|k}) > \text{tr}(\mathbf{P}_{k|k-1})$ **then**
- 13: $\hat{\mathbf{x}}_{k|k} = \hat{\mathbf{x}}_{k|k-1}$
- 14: $\mathbf{P}_{k|k} = \mathbf{P}_{k|k-1}$
- 15: **end if**
- 16: **end for**

where, $\hat{\mathbf{x}}$ is the estimated states, \mathbf{P} is the states' covariance matrix, $\hat{\mathbf{y}}$ is the estimated measurements, \mathbf{P}_{xy} is the covariance between the states and the measurements, \mathbf{P}_y is the covariance of the estimated measurements, \mathbf{S} is the innovation (or residual) covariance, \mathbf{K} is the Kalman gain. The subscript $k|k-1$ represents the estimated value before the state update, and $k|k$ represents the estimated value after the state update.

Fig. 2. The proposed framework for nonlinear KFs. Note that the framework degrades to the old framework when rows 9–15 are replaced by (Eq. 7).

Simulation results

To demonstrate the effectiveness of the proposed framework, we validated it in five different applications suitable for nonlinear KFs. A brief description of the five applications is presented in Table 1, and a detailed description of the system models and parameter setup can be found in the Materials and Methods section. For each scenario, we combined the old and proposed framework with four different types of nonlinear KFs: EKF, EKF2, UKF, and CKF. We also implemented the IEKF for comparison. The detailed EKF, EKF2, UKF, CKF, and IEKF algorithms used in the paper can be found in Figs. S1–5. All these nine (4 + 4 + 1) nonlinear KFs are used for state estimation under different measurement noise setups (the covariance of the measurement noises differs in different setups). To guarantee the fairness of the comparison and reduce the effect of randomness, each KF is simulated 10,000 times for each measurement noise setup, and all the KFs use the same random seed during the simulation. This means that the random initial states' errors, random process noises, and random measurement noises are the same for the i^{th} simulation of EKF and the i^{th} simulation of UKF. In other words, all these random noises were generated for the 10,000 runs *a priori* and recalled for simulating each estimation method.

Table 1. A brief description of the five applications of nonlinear Kalman filters investigated in this paper. Note that all five applications have nonlinear measurement functions to demonstrate the effectiveness of the new framework proposed in this paper.

Applications	3D target tracking	Terrain-referenced navigation	Synchronous generator state estimation	Pendulum state estimation	Battery state estimation
Number of states	6	2	4	2	3
Linear state transition function?	Yes	Yes	No	No	No
Number of measurements	2	1	1	1	1
Linear measurement functions?	No	No	No	No	No
Number of inputs	3	2	3	1	1
Number of iterations	30	100	100	100	180

The root mean squared error (RMSE) of the state estimations given by different nonlinear KFs are shown in Fig. 3 and Figs. S6–9. Note that we only showed the RMSE of two representative states for systems with more than two states. For example, in 3D target tracking, the six states are the object’s speed and position along the three axes, and Fig. 3 examines the object’s speed and position estimation accuracy along the x-axis. As can be seen from the five figures, the simulation results are very similar to each other. Therefore, only the results of the first task, 3D target tracking, are analyzed in depth in this section.

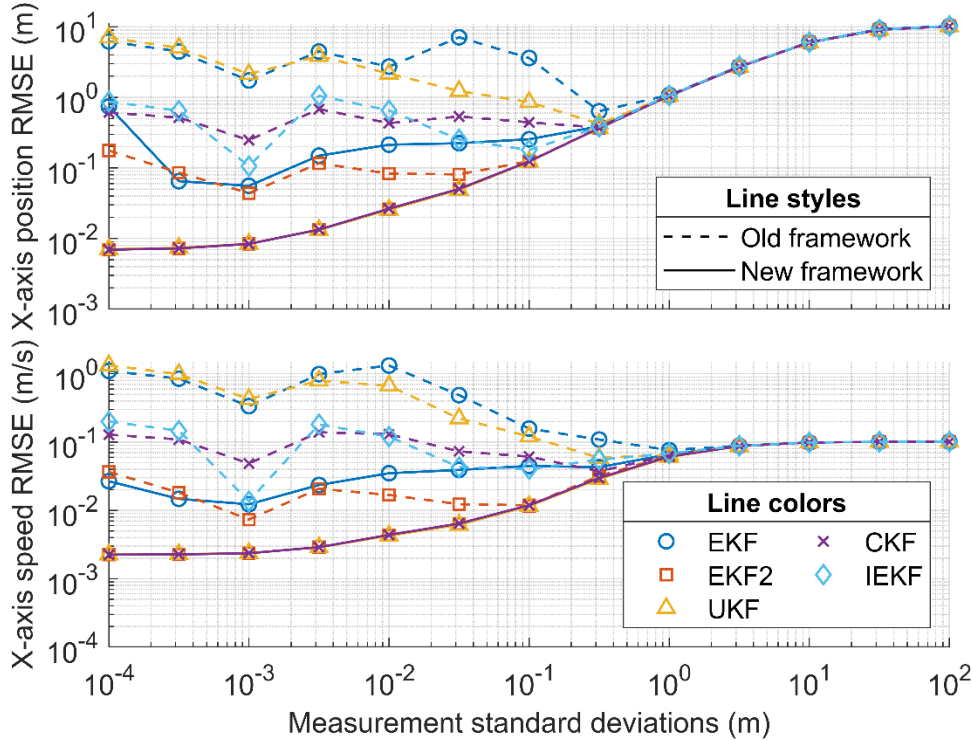


Fig. 3. The root mean squared error of the state estimations under different measurement noise setups (3D target tracking). Different types of nonlinear Kalman filters are represented by different colors and markers, while the old and new frameworks are represented by dotted lines and solid lines, respectively. The x-axis represents the standard deviations of the two distance sensors. The root mean squared error is calculated from the estimation errors in 10,000 simulations. The estimation error is calculated as the difference between the estimated state and the true state at the end of the final iteration of each simulation.

As shown in Fig 3, the proposed framework (solid lines) significantly improves the accuracy of all types of nonlinear Kalman filters. The improvement becomes stronger as the measurement noise becomes smaller. This result aligns with our expectations because the proposed framework only changes how the measurements are used in the nonlinear KF, and the estimations will rely more on the measurements instead of system knowledge as the measurement noise decreases. When the standard deviations of the two

measurements are both less than 0.01 meters, the RMSE of all four types of nonlinear KFs can be reduced by about one to three orders of magnitude, which is a significant improvement.

Another interesting observation of Fig. 3 and Figs. S6–9 is that the RMSE of EKF2, UKF, and CKF becomes quite similar after the new framework is used. This phenomenon can be explained by the fact that all three methods consider the first and second-order terms in the Taylor expansion of the nonlinear state transition and/or measurement functions in certain ways (12). On the other hand, EKF is generally slightly worse than the other three types of nonlinear KFs because it only considers the first-order terms in the Taylor expansion.

By comparing the performance of IEKF and EKF (with and without the new framework) in Fig. 3 and Figs. S6–9, we can see that IEKF does perform better than EKF with the old framework, yet it is almost always worse than EKF with the new framework despite requiring longer computational time. As we mentioned in the Introduction, the main reason for such a difference is that IEKF can still give overconfident covariance estimation when it fails to converge, which happens quite often in practice.

As we mentioned in the introduction, the fundamental idea of the proposed framework is to make a more accurate covariance estimation by re-approximating the measurement functions after the state update. To validate if the covariance estimation really becomes more accurate in the new framework, we compared the actual and estimated RMSE of the x-axis position (the first state in the system) in the old and new framework in Fig. 3. In the figure, for each type of nonlinear KF (represented by different line colors) and framework (the old and new frameworks are respectively shown in the top and bottom subfigures), the closeness between the actual RMSE (the solid line) and estimated RMSE (dotted line) represents the accuracy of the state covariance estimation. Apparently, when the standard deviations of the two measurements are lower than 0.1 meters, the conventional framework always significantly underestimates the covariance, sometimes by several orders of magnitude, regardless of the type of nonlinear KF used. On the other hand, for the new framework, only the RMSE of EKF is underestimated, and the covariance estimation of other types of nonlinear KFs matches the actual value very well. This, again, can be explained by the fact that EKF neglects the second and higher-order information of the measurement functions, so its covariance estimation is less accurate than other methods. Yet still, the covariance estimation of EKF becomes much more precise when combined with the new framework.

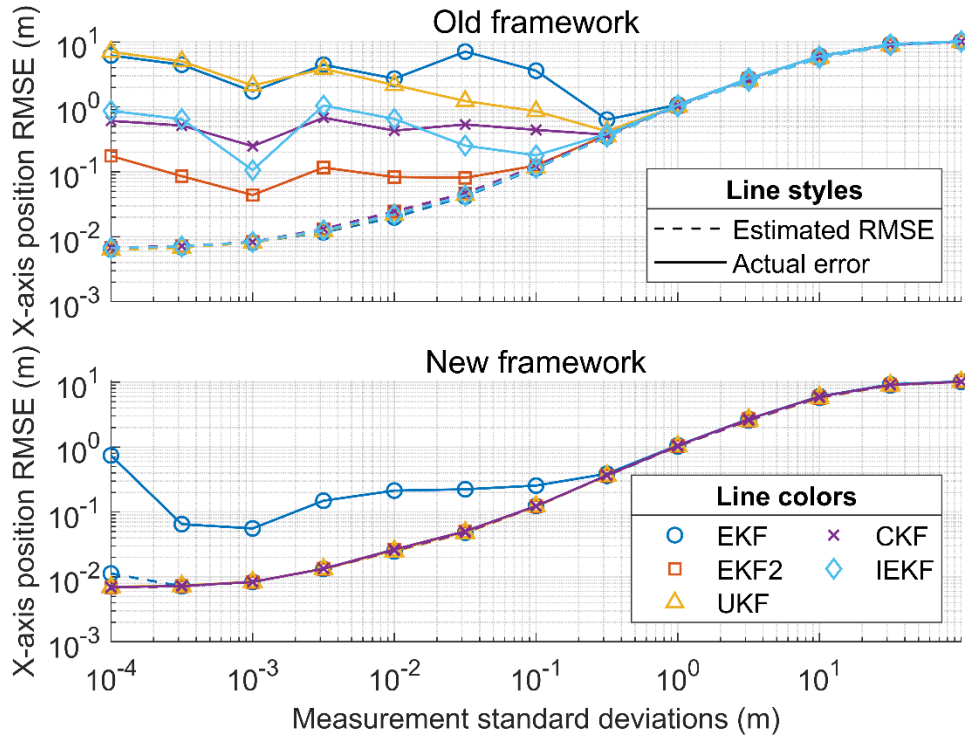


Fig. 4. The actual and estimated root mean squared error of the x-axis position estimation. Different types of nonlinear Kalman filters are represented by different colors and markers, while the estimated and actual root mean squared errors are represented by dotted lines and solid lines, respectively. The x-axis represents the standard deviations of the two distance sensors. Both root mean squared errors are calculated from the estimation errors in 10,000 simulations. The actual estimation error is calculated as the difference between the estimated state and the true state at the end of the final iteration of each simulation. The estimated estimation error is calculated as the square root of the estimated variance of the state at the end of the final iteration of each simulation.

Another interesting observation of Fig. 4 is that the estimated RMSE of the x-axis position (the dashed lines) is actually very similar for different combinations of frameworks and KFs. This suggests that the accuracy of the estimation mainly relates to whether the covariance estimation is accurate or not, which leads to the conclusion mentioned at the end of the Introduction – to achieve a more accurate estimation, finding the optimal Kalman gain is not as important as accurately estimating the covariance.

Another important metric for evaluating the performance of different filters is the convergence characteristics. We visualized this metric by fixing the standard deviations of the two measurements to 0.01 m and plotted the RMSE of the state estimations after different numbers of iterations. The results are shown in Fig. 5. From the figure, we can see that all types of nonlinear KFs can converge faster after being combined with the new framework. This result suggests that the proposed framework is very suitable for applications that require high convergence speed.

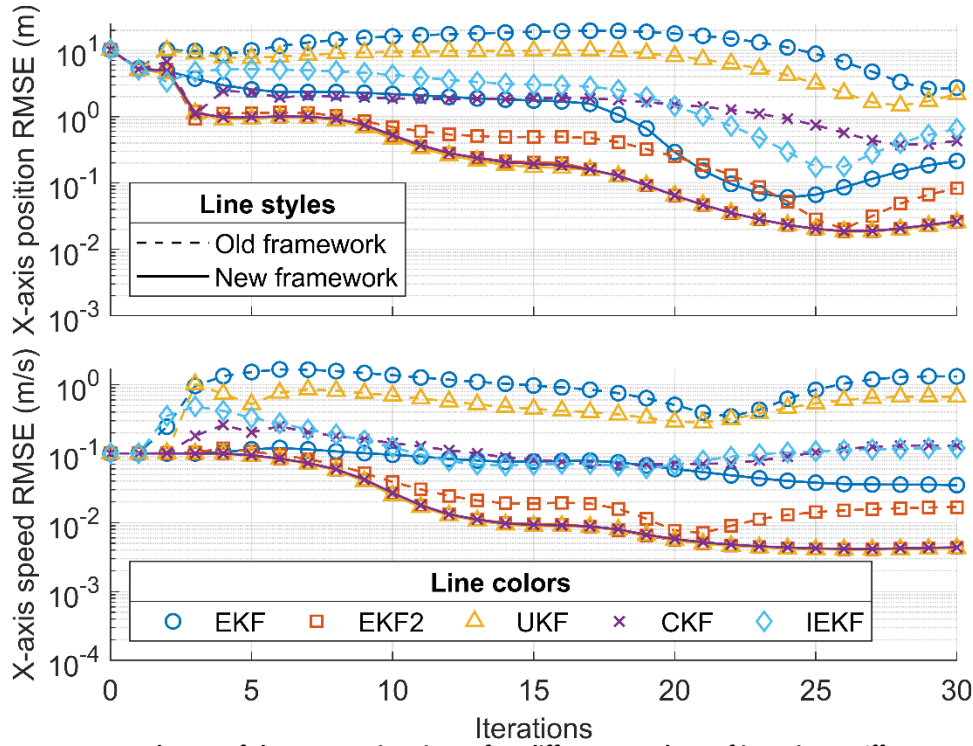


Fig. 5. The root mean squared error of the state estimations after different numbers of iterations. Different types of nonlinear Kalman filters are represented by different colors and markers, while the old and new frameworks are represented by dotted lines and solid lines, respectively. The standard deviations of the two measurements are fixed to be 0.01 m. The root mean squared error after k iterations is calculated from the estimation errors after k iterations in 10,000 simulations. The estimation error after k iterations is calculated as the difference between the estimated state and the true state at the end of the k^{th} iteration of each simulation.

Since the extra steps introduced in the new framework take time, it is also important to compare the computational time of the two frameworks. The results are summarized in Fig. 6. In general, the new framework increases the computational time by 10–90%, varying for different nonlinear systems. Namely, when the system has linear state transition functions and nonlinear measurement functions (which is true for the first two applications in the table), then the “update” step should be accountable for most of the computational time in the conventional framework and re-approximating the measurement functions can almost double the runtime in the worst case. The additional runtime is related to the type of nonlinear KF as well. In UKF and CKF, one of the most time-consuming steps is to calculate the square root of the state covariance matrix. This step is respectively done one, two, two, and three times in each iteration of UKF (old framework), UKF (new framework), CKF (old framework), and CKF (new framework). Therefore, the computational time increase (in percentage) brought by the new framework is longer for UKF than for CKF. Noticing that the new framework can reduce the estimation error by more than an order of magnitude when the measurement noise is small, we can say that the extra computational complexity is generally worth it. Another thing to note is that the combination of EKF and the new framework requires significantly less computational time than the combination of any other nonlinear KFs and the old framework. At the same time, the former’s accuracy is generally higher than the latter in the applications we examined in this paper. Therefore, even in situations where the computational time is of major concern, the proposed framework can still be helpful in the sense that the new EKF can outperform the old EKF2, UKF, and CKF, in addition to saving a lot of computational time.

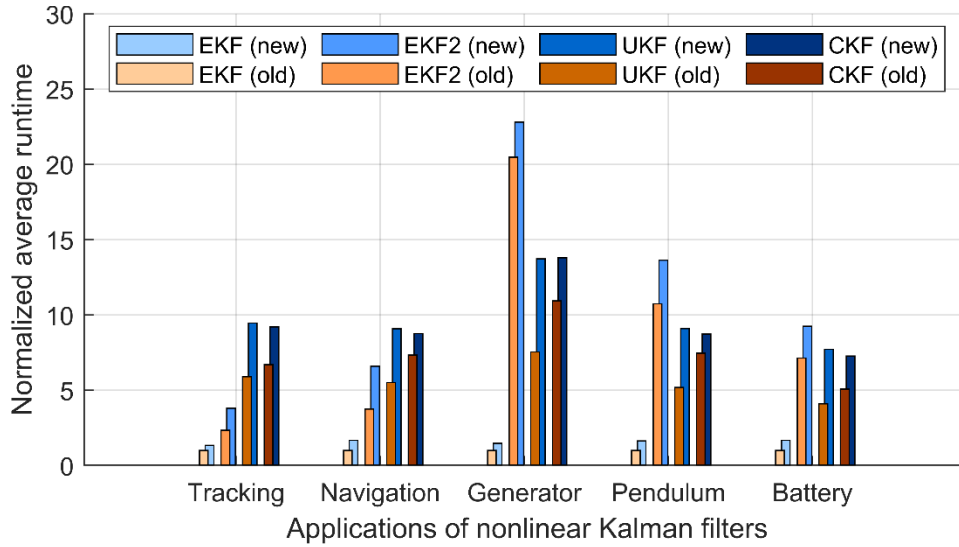


Fig. 6. Comparison of the computational time of different methods and frameworks. The average runtime shown in the figure is calculated from over 100,000 simulations run on the same computer. Specifically, for each combination of nonlinear Kalman filter and framework, we record the method's runtime whenever it is used and calculate the average in the end. After the average runtime is calculated, the value is normalized with respect to the average runtime of the conventional extended Kalman filter for the same application. In other words, the normalized average runtime of "EKF (old)" always equals one in the figure. The applications examined here are 3D target tracking, terrain-referenced navigation, synchronous generator state estimation, pendulum state estimation, and battery state estimation.

DISCUSSION

In this paper, we proposed a new framework that can be applied to all types of nonlinear KFs. The new framework re-approximates the measurement functions after the state update, solving the problem of overconfident state covariance estimation, which is an inherent problem in the conventional framework for nonlinear KFs. The new framework was tested in five different applications, reducing the estimation errors by more than an order of magnitude when the measurement noise is low and significantly reducing the convergence time of the algorithm. Considering that all types of sensors will become increasingly more accurate in the future, the proposed framework can also bring greater benefits for all kinds of nonlinear KFs over time.

The main limitation of this work is that the proposed framework can only be used in discrete-time nonlinear KFs. For continuous-time nonlinear KFs, the state estimations change continuously over time, so the problem of overconfident covariance estimation does not exist. However, all digital sensors in real life give discrete-time measurements. Even though it is possible to make the signals continuous through interpolation, the continuous-time state estimation problem sometimes includes several partial differential equations, so it is hard and takes a long time to solve (19). Therefore, most applications of nonlinear KFs in real life use the discrete-time form, and they can all benefit from the new framework proposed in this paper.

MATERIALS AND METHODS

This paper uses five different applications of nonlinear KFs to test the effectiveness of the new framework: 3D target tracking, terrain-referenced navigation, synchronous generator state estimation, pendulum state estimation, and battery state estimation.

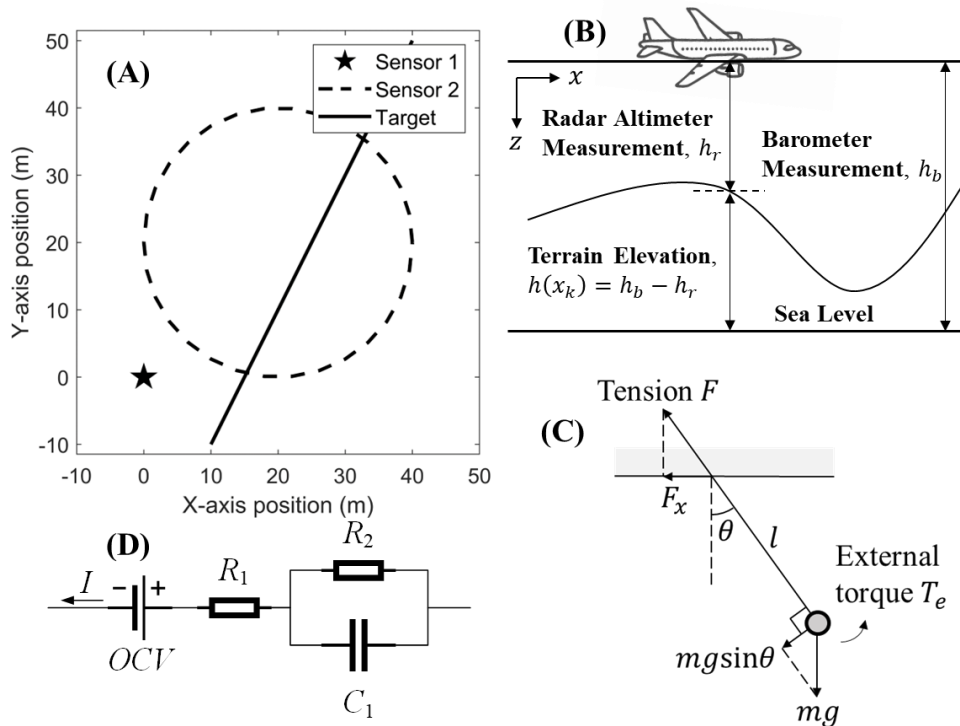


Fig. 7. Examples of nonlinear systems used to validate the proposed framework in this paper. (A) 3D object tracking. (B) Terrain-referenced navigation. (C) Pendulum state estimation. (D) Battery state estimation.

3D target tracking

This example is adapted from Example 3.3.1 in (20). As shown in Fig. 7A, a target is moving in space, and two sensors are used to track its location. The first sensor is at the origin, and the second sensor moves in a circle. The second sensor's location (x_{s1}, x_{s2}, x_{s3}) at step $k = 1, 2, \dots, 30$ is represented by:

$$\begin{cases} x_{s1,k} = 20 + 20 \cos\left(\frac{(k-1)\pi}{15}\right) \\ x_{s2,k} = 20 + 20 \sin\left(\frac{(k-1)\pi}{15}\right) \\ x_{s3,k} = 0 \end{cases} \quad (9)$$

The states are the target's positions (x_1, x_2, x_3) and speeds (v_1, v_2, v_3) along the three axes. The measurements y_1, y_2 are the distances between the target and the two sensors. The inputs are the target's accelerations along the three axes, which are assumed to be zero in this example. When the time interval is set to $\Delta t = 1$ s, the system's state transition and measurement functions can be written as (Eq. 10). Note that the noises are omitted in the equations.

$$\begin{aligned}
\begin{bmatrix} x_{1,k} \\ x_{2,k} \\ x_{3,k} \\ v_{1,k} \\ v_{2,k} \\ v_{3,k} \end{bmatrix} &= \begin{bmatrix} x_{1,k-1} + v_{1,k-1} \\ x_{2,k-1} + v_{2,k-1} \\ x_{3,k-1} + v_{3,k-1} \\ v_{1,k-1} \\ v_{2,k-1} \\ v_{3,k-1} \end{bmatrix} \\
\begin{bmatrix} y_{1,k} \\ y_{2,k} \end{bmatrix} &= \begin{bmatrix} \sqrt{x_{1,k}^2 + x_{2,k}^2 + x_{3,k}^2} \\ \sqrt{(x_{1,k} - x_{s1,k})^2 + (x_{2,k} - x_{s2,k})^2 + (x_{3,k} - x_{s3,k})^2} \end{bmatrix}
\end{aligned} \tag{10}$$

The true initial states of the target are $x_{1,0} = 10, x_{2,0} = -10, x_{3,0} = 50, v_{1,0} = 1, v_{2,0} = 2, v_{3,0} = 0$; the initial state covariance matrix P_0 is diagonal, and its diagonal elements are 100, 100, 100, 0.01, 0.01, and 0.01. The initial state estimations are generated randomly from the multivariate Gaussian distribution with covariance P_0 and mean equal to the true initial states. The initial process noise covariance matrix P_0 is also diagonal, and its diagonal values are 0, 0, 0, $1e-6$, $1e-6$, and $1e-6$.

Terrain-referenced navigation

This example is adapted from Example 3.3.2 in (20). As shown in Fig. 7B, a plane flies above an uneven landscape. The states are the planes' positions along the two axes, which are denoted as x_1 and x_2 . The measurement y_k is the terrain's elevation at the plane's present location, which, in practice, is calculated as the difference between the barometer and radar altimeter measurements. The plane knows the contour map in advance, so the terrain's elevation can tell the aircraft its possible locations. However, this task is difficult because all the points on a contour line have the same elevation, and system knowledge must be combined for accurate state estimations. The system inputs are the plane's speeds along the x and y axes, which are 0.5 km/s and 0, respectively. When the time interval is set to $\Delta t = 1$ s, the system's state transition and measurement functions can be written as (Eq. 11). Note that all the units for distance in this example are kilometers, and the noises are omitted in the equations.

$$\begin{aligned}
\begin{bmatrix} x_{1,k} \\ x_{2,k} \end{bmatrix} &= \begin{bmatrix} x_{1,k-1} + 0.5 \\ x_{2,k-1} \end{bmatrix} \\
y_k &= 1000 \sin \sqrt{\left(\frac{x_{1,k}}{40}\right)^2 + \left(\frac{x_{2,k}}{40}\right)^2}
\end{aligned} \tag{11}$$

The true initial states of the target are $x_{1,0} = 10, x_{2,0} = 10$; the initial state covariance matrix P_0 is diagonal, and its diagonal elements are ones. The initial state estimations are generated randomly from the multivariate Gaussian distribution with covariance P_0 and

mean equal to the true initial states. The process noise covariance matrix is also diagonal, and its diagonal values are both $2.5\text{e-}7$.

Synchronous generator state estimation

This example is adapted from a research paper (21). The system model is precisely the same as in the paper. The states of the system are the rotor angle δ , rotor speed $\Delta\omega$, the q-axis component of the voltage e'_q , and the d-axis component of the voltage e'_d . For simplicity, these states are denoted as $x_1 \sim x_4$. The measurement y_k is electrical output power. The system's inputs include the mechanical input torque T_m , the steady-state internal voltage of the armature E_{fd} , and the terminal bus voltage V_t . For simplicity, these inputs are denoted as $u_1 \sim u_3$. The time interval is set to $\Delta t = 0.1$ ms. The input profiles are the same as in the paper, which are:

$$\begin{cases} u_{1,k} = 0.8 \\ u_{2,k} = 2.11 + 0.0002k \\ u_{3,k} = 1.002 \end{cases} \quad (12)$$

All the model parameters are selected to be the same as in (21). The system's state transition and measurement functions can be written as (Eq. 13). Note that the noises are omitted from the equations.

$$\begin{bmatrix} x_{1,k} \\ x_{2,k} \\ x_{3,k} \\ x_{4,k} \end{bmatrix} = \begin{bmatrix} x_{1,k-1} + 377x_{2,k-1}\Delta t \\ x_{2,k-1} + \frac{\Delta t}{13} \left[u_{1,k-1} - \frac{u_{3,k-1}x_{3,k-1} \sin x_{1,k-1}}{0.375} + 0.9215u_{3,k-1}^2 \sin(2x_{1,k-1}) - 0.05x_{2,k-1} \right] \\ x_{3,k-1} + \frac{\Delta t}{0.131} \left[u_{2,k-1} - x_{3,k-1} - 4.4933(x_{3,k-1} - u_{3,k-1} \cos x_{1,k-1}) \right] \\ x_{4,k-1} + \frac{\Delta t}{0.0131} \left[-x_{4,k-1} + 0.6911u_{3,k-1} \sin x_{1,k-1} \right] \end{bmatrix}$$

$$y_k = \frac{u_{3,k-1}x_{3,k} \sin x_{1,k}}{0.375} + 0.9215u_{3,k-1}^2 \sin(2x_{1,k}) \quad (13)$$

The true initial states of the system are $x_{1,0} = 0.4, x_{2,0} = x_{3,0} = x_{4,0} = 0$. The initial state covariance matrix P_0 is diagonal, and its diagonal elements are $1\text{e-}4, 1\text{e-}10, 1\text{e-}4$, and $1\text{e-}4$. The initial state estimations are generated randomly from the multivariate Gaussian distribution with covariance P_0 and mean equal to the true initial states. The process noise covariance matrix is also diagonal, and its diagonal values are $1\text{e-}10, 1\text{e-}16, 1\text{e-}10$, and $1\text{e-}10$.

Pendulum state estimation

As shown in Fig. 7C, one end of the pendulum is fixed to the ceiling with a thin rope. The system's states are the pendulum's angular position θ and angular speed ω . The

measurement y_k is the horizontal component of tension in the rope. The system input is the external torque exerted on the pendulum, which is zero in this example. The mass of the ball is $m = 1$ kg, the length of the rope is $l = 1$ m, and the gravity acceleration is $g = 9.8$ m/s². The time interval is set to $\Delta t = 0.01$ s. According to Newton's law, when the time interval is small, the system's state transition and measurement functions can be written as (Eq. 14). Note that the noises are omitted in the equations.

$$\begin{bmatrix} \omega_k \\ \theta_k \end{bmatrix} = \begin{bmatrix} \omega_{k-1} - \frac{g}{l} \sin(\theta_{k-1}) \Delta t \\ \theta_{k-1} + \omega_{k-1} \Delta t \end{bmatrix} \quad (14)$$

$$y_k = mg \cos \theta_k \sin \theta_k + ml \omega_k^2 \sin \theta_k$$

The true initial states of the system are $\omega_0 = 0, \theta_0 = \pi / 4$. The initial state covariance matrix P_0 is diagonal, and its diagonal elements are both $(\pi / 18)^2$. The initial state estimations are generated randomly from the multivariate Gaussian distribution with covariance P_0 and mean equal to the true initial states. The process noise covariance matrix is also diagonal; its diagonal values are $1e-10$ and 0 .

Battery state estimation

This example is adapted from a research paper (22). As shown in Fig. 7D, a battery can be modeled as several circuit components, including a voltage source OCV (stands for the cell's open-circuit voltage), an internal resistor R_1 , a transfer resistor R_2 , and a capacitor C_1 . A battery's two most important states are its state of charge (SOC) and state of health (SOH). The SOC is the ratio of the battery's remaining capacity to its present maximum capacity, and the SOH is the ratio of the battery's present maximum capacity to its initial maximum capacity. In general, SOC describes the battery's energy level, while SOH describes the battery's aging level. The states of this system are the SOC, SOH, and capacitor voltage U_c . The measurement y_k is the battery's terminal voltage. The input is the charging current, which, in this example, is a 3-level square wave shown below:

$$I_k = \begin{cases} -2, & 75 \geq k > 15 \\ 2, & 165 \geq k > 105 \\ 0, & \text{else} \end{cases} \quad (15)$$

The battery's initial maximum capacity is $Q_0 = 1$ Ah. The parameters in the equivalent circuit model are chosen to be $R_1 = 0.08, R_2 = 0.05, 1/(R_2 C_1) = 0.008$. The OCV is a function of SOC and SOH, and it can be written as:

$$OCV = \sum_{i=0}^9 \left(\frac{SOH - 0.8}{0.2} a_{100,i+1} + \frac{1 - SOH}{0.2} a_{80,i+1} \right) SOC^i$$

$$a_{100} = [1390.38, -6961.31, 14760.31, -17230.92, 12055.71, -5162.75, 1330.60, -196.37, 15.60, 2.96] \quad (16)$$

$$a_{80} = [813.94, -4229.96, 9345.49, -11415.388396.15, -3801.07, 1043.09, -165.29, 14.28, 2.96]$$

The time interval is set to $\Delta t = 1$ s, and the total simulation time is 180 seconds. The system's state transition and measurement functions can be written as (Eq. 17). Note that the noises are omitted in the equations.

$$\begin{bmatrix} SOC_k \\ U_{c,k} \\ SOH_k \end{bmatrix} = \begin{bmatrix} SOC_{k-1} + \frac{I_{k-1} \Delta t}{3600 Q_0 SOH_{k-1}} \\ U_{c,k-1} \exp\left(\frac{-\Delta t}{R_2 C_1}\right) + \left(1 - \exp\left(\frac{-\Delta t}{R_2 C_1}\right)\right) R_2 I_{k-1} \\ SOH_{k-1} \end{bmatrix} \quad (17)$$

$$y_k = OCV(SOC_k, SOH_k) + U_{c,k} + R_1 I_k$$

The true initial states of the system are $SOC_0 = 60\%$, $U_{c,0} = 0$, $SOH_0 = 90\%$. The initial state covariance matrix P_0 is diagonal; its diagonal elements are 0.04, $1e-10$, and 0.01. The initial state estimations are 80%, 0, and 100%, respectively. The input current is noisy, and its standard deviation is 1 mA. This input noise is the only source of the process noises. Since the input current also appears in the measurement function, the actual measurement noise is the combination of the measurement noise of the voltmeter and the noise caused by the term $R_1 I_k$ in the measurement function.

Supplementary Materials

Supplementary figures

Input: Process noise covariance matrix \mathbf{Q}_k , Measurement noise covariance matrix \mathbf{R}_k , state transition function $\mathbf{f}(\mathbf{x}, \mathbf{u})$, measurement function $\mathbf{h}(\mathbf{x})$, system inputs \mathbf{u}_k , measurements \mathbf{z}_k

Initialization:

- 1: $\hat{\mathbf{x}}_{0|0} = \mathbb{E}[\mathbf{x}_0]$
- 2: $\mathbf{P}_{0|0} = \mathbb{E}[(\hat{\mathbf{x}}_{0|0} - \mathbf{x}_0)(\hat{\mathbf{x}}_{0|0} - \mathbf{x}_0)^T]$
- 3: **for** every time step k **do**
- Predict:**
- 4: $\mathbf{F}_k = \frac{\partial \mathbf{f}}{\partial \mathbf{x}}|_{\hat{\mathbf{x}}_{k-1|k-1}, \mathbf{u}_{k-1}}$
- 5: $\hat{\mathbf{x}}_{k|k-1} = \mathbf{f}(\hat{\mathbf{x}}_{k-1|k-1}, \mathbf{u}_{k-1})$
- 6: $\mathbf{P}_{k|k-1} = \mathbf{F}_k \mathbf{P}_{k-1|k-1} \mathbf{F}_k^T + \mathbf{Q}_k$
- Update:**
- 7: $\mathbf{H}_{k|k-1} = \frac{\partial \mathbf{h}}{\partial \mathbf{x}}|_{\hat{\mathbf{x}}_{k|k-1}}$
- 8: $\hat{\mathbf{y}}_{k|k-1} = \mathbf{h}(\hat{\mathbf{x}}_{k|k-1})$
- 9: $\mathbf{P}_{xy,k|k-1} = \mathbf{P}_{k|k-1} \mathbf{H}_{k|k-1}^T$
- 10: $\mathbf{P}_{y,k|k-1} = \mathbf{H}_{k|k-1} \mathbf{P}_{k|k-1} \mathbf{H}_{k|k-1}^T$
- 11: $\mathbf{S}_{k|k-1} = \mathbf{P}_{y,k|k-1} + \mathbf{R}_k$
- 12: $\mathbf{K} = \mathbf{P}_{xy,k|k-1} \mathbf{S}_{k|k-1}^{-1}$
- 13: $\hat{\mathbf{x}}_{k|k} = \hat{\mathbf{x}}_{k|k-1} + \mathbf{K}(\mathbf{z}_k - \hat{\mathbf{y}}_{k|k-1})$
- Recalibrate:**
- 14: $\mathbf{H}_{k|k} = \frac{\partial \mathbf{h}}{\partial \mathbf{x}}|_{\hat{\mathbf{x}}_{k|k}}$
- 15: $\mathbf{P}_{xy,k|k} = \mathbf{P}_{k|k-1} \mathbf{H}_{k|k}^T$
- 16: $\mathbf{P}_{y,k|k} = \mathbf{H}_{k|k} \mathbf{P}_{k|k-1} \mathbf{H}_{k|k}^T$
- 17: $\mathbf{S}_{k|k} = \mathbf{P}_{y,k|k} + \mathbf{R}_k$
- 18: $\mathbf{P}_{k|k} = \mathbf{P}_{k|k-1} + \mathbf{K} \mathbf{S}_{k|k} \mathbf{K}^T - \mathbf{P}_{xy,k|k} \mathbf{K}^T - \mathbf{K} \mathbf{P}_{xy,k|k}^T$
- Back out:**
- 19: **if** $\text{tr}(\mathbf{P}_{k|k}) > \text{tr}(\mathbf{P}_{k|k-1})$ **then**
- 20: $\hat{\mathbf{x}}_{k|k} = \hat{\mathbf{x}}_{k|k-1}$
- 21: $\mathbf{P}_{k|k} = \mathbf{P}_{k|k-1}$
- 22: **end if**
- 23: **end for**

Fig. S1. The implementation of the new framework on the extended Kalman filter. Note that rows 14–22 are replaced by (Eq. 7) in the conventional framework.

Algorithm 5 The second-order extended Kalman filter with the new framework

Input: Process noise covariance matrix \mathbf{Q}_k , Measurement noise covariance matrix \mathbf{R}_k , states number n_x , measurements number n_m , state transition function $\mathbf{f}(\mathbf{x}, \mathbf{u})$, measurement function $\mathbf{h}(\mathbf{x})$, system inputs \mathbf{u}_k , measurements \mathbf{z}_k

Initialization:

- 1: $\hat{\mathbf{x}}_{0|0} = \mathbb{E}[\mathbf{x}_0]$
 - 2: $\mathbf{P}_{0|0} = \mathbb{E}[(\hat{\mathbf{x}}_{0|0} - \mathbf{x}_0)(\hat{\mathbf{x}}_{0|0} - \mathbf{x}_0)^T]$
 - 3: **for** every time step k **do**
 - Predict:**
 - 4: $\mathbf{F}_k = \frac{\partial \mathbf{f}}{\partial \mathbf{x}}|_{\hat{\mathbf{x}}_{k-1|k-1}, \mathbf{u}_{k-1}}$
 - 5: $\mathbf{F}_{i,k}^* = \left[\frac{\partial^2 f_i}{\partial x_m \partial x_n} |_{\hat{\mathbf{x}}_{k-1|k-1}, \mathbf{u}_{k-1}} \right]_{mm}, i = 1, \dots, n_x$
 - 6: $\hat{\mathbf{x}}_{k|k-1} = \mathbf{f}(\hat{\mathbf{x}}_{k-1|k-1}, \mathbf{u}_{k-1}) + \frac{1}{2} [\text{tr}(\mathbf{F}_{i,k}^* \mathbf{P}_{k-1|k-1})]_i$
 - 7: $\mathbf{P}_{k|k-1} = \mathbf{F}_k \mathbf{P}_{k-1|k-1} \mathbf{F}_k^T + \frac{1}{2} [\text{tr}(\mathbf{F}_{i,k}^* \mathbf{P}_{k-1|k-1} \mathbf{F}_{j,k}^* \mathbf{P}_{k-1|k-1})]_{ij} + \mathbf{Q}_k$
 - Update:**
 - 8: $\mathbf{H}_{k|k-1} = \frac{\partial \mathbf{h}}{\partial \mathbf{x}}|_{\hat{\mathbf{x}}_{k|k-1}}$
 - 9: $\mathbf{H}_{i,k|k-1}^* = \left[\frac{\partial^2 h_i}{\partial x_m \partial x_n} |_{\hat{\mathbf{x}}_{k|k-1}} \right]_{mm}, i = 1, \dots, n_m$
 - 10: $\hat{\mathbf{y}}_{k|k-1} = \mathbf{h}(\hat{\mathbf{x}}_{k|k-1}) + \frac{1}{2} [\text{tr}(\mathbf{H}_{i,k|k-1}^* \mathbf{P}_{k|k-1})]_i$
 - 11: $\mathbf{P}_{xy,k|k-1} = \mathbf{P}_{k|k-1} \mathbf{H}_{k|k-1}^T$
 - 12: $\mathbf{P}_{y,k|k-1} = \mathbf{H}_{k|k-1} \mathbf{P}_{k|k-1} \mathbf{H}_{k|k-1}^T + \frac{1}{2} [\text{tr}(\mathbf{H}_{i,k|k-1}^* \mathbf{P}_{k|k-1} \mathbf{H}_{j,k|k-1}^* \mathbf{P}_{k|k-1})]_{ij}$
 - 13: $\mathbf{S}_{k|k-1} = \mathbf{P}_{y,k|k-1} + \mathbf{R}_k$
 - 14: $\mathbf{K} = \mathbf{P}_{xy,k|k-1} \mathbf{S}_{k|k-1}^{-1}$
 - 15: $\hat{\mathbf{x}}_{k|k} = \hat{\mathbf{x}}_{k|k-1} + \mathbf{K}(\mathbf{z}_k - \hat{\mathbf{y}}_{k|k-1})$
 - Recalibrate:**
 - 16: $\mathbf{H}_{k|k} = \frac{\partial \mathbf{h}}{\partial \mathbf{x}}|_{\hat{\mathbf{x}}_{k|k}}$
 - 17: $\mathbf{H}_{i,k|k}^* = \left[\frac{\partial^2 h_i}{\partial x_m \partial x_n} |_{\hat{\mathbf{x}}_{k|k}} \right]_{mm}, i = 1, \dots, n_m$
 - 18: $\mathbf{P}_{xy,k|k} = \mathbf{P}_{k|k-1} \mathbf{H}_{k|k}^T$
 - 19: $\mathbf{P}_{y,k|k} = \mathbf{H}_{k|k} \mathbf{P}_{k|k-1} \mathbf{H}_{k|k}^T + \frac{1}{2} [\text{tr}(\mathbf{H}_{i,k|k}^* \mathbf{P}_{k|k-1} \mathbf{H}_{j,k|k}^* \mathbf{P}_{k|k-1})]_{ij}$
 - 20: $\mathbf{S}_{k|k} = \mathbf{P}_{y,k|k} + \mathbf{R}_k$
 - 21: $\mathbf{P}_{k|k} = \mathbf{P}_{k|k-1} + \mathbf{K} \mathbf{S}_{k|k} \mathbf{K}^T - \mathbf{P}_{xy,k|k} \mathbf{K}^T - \mathbf{K} \mathbf{P}_{xy,k|k}^T$
 - Back out:**
 - 22: **if** $\text{tr}(\mathbf{P}_{k|k}) > \text{tr}(\mathbf{P}_{k|k-1})$ **then**
 - 23: $\hat{\mathbf{x}}_{k|k} = \hat{\mathbf{x}}_{k|k-1}$
 - 24: $\mathbf{P}_{k|k} = \mathbf{P}_{k|k-1}$
 - 25: **end if**
 - 26: **end for**
-

Fig. S2. The implementation of the new framework on the second-order extended Kalman filter. Note that rows 16–25 are replaced by (Eq. 7) in the conventional framework.

Input: Process noise covariance matrix \mathbf{Q}_k , Measurement noise covariance matrix \mathbf{R}_k , states number n_x , state transition function $\mathbf{f}(\mathbf{x}, \mathbf{u})$, measurement function $\mathbf{h}(\mathbf{x})$, system inputs \mathbf{u}_k , measurements \mathbf{z}_k , hyperparameters $\alpha = 10^{-3}, \beta = 2, \kappa = 0$

Initialization:

- 1: $\hat{\mathbf{x}}_{0|0} = \mathbb{E}[\mathbf{x}_0]$
 - 2: $\mathbf{P}_{0|0} = \mathbb{E}[(\hat{\mathbf{x}}_{0|0} - \mathbf{x}_0)(\hat{\mathbf{x}}_{0|0} - \mathbf{x}_0)^T]$
 - 3: $\lambda = \alpha^2(n_x + \kappa) - n_x$
 - 4: $W_i^{(c)} = W_i^{(m)} = 1/(2n_x + 2\lambda), i = 1, \dots, n_x$
 - 5: $W_0^{(c)} = \lambda/(n_x + \lambda) + 1 - \alpha^2 + \beta$
 - 6: $W_0^{(m)} = \lambda/(n_x + \lambda)$
 - 7: **for** every time step k **do**
 - Predict:**
 - 8: $\mathbf{L}_i = [\sqrt{\mathbf{P}_{k-1|k-1}}]_i, i = 1, \dots, n_x$
 - 9: $\mathcal{X}_{0,k-1} = \hat{\mathbf{x}}_{k-1|k-1}$
 - 10: $\mathcal{X}_{i,k-1} = \hat{\mathbf{x}}_{k-1|k-1} + \sqrt{\lambda + n_x} \mathbf{L}_i, i = 1, \dots, n_x$
 - 11: $\mathcal{X}_{i+n_x,k-1} = \hat{\mathbf{x}}_{k-1|k-1} - \sqrt{\lambda + n_x} \mathbf{L}_i, i = 1, \dots, n_x$
 - 12: $\mathcal{X}_{i,k|k-1} = \mathbf{f}(\mathcal{X}_{i,k-1}, \mathbf{u}_{k-1}), i = 0, 1, \dots, 2n_x$
 - 13: $\hat{\mathbf{x}}_{k|k-1} = \sum_{i=0}^{2n_x} W_i^{(m)} \mathcal{X}_{i,k|k-1}$
 - 14: $\mathbf{P}_{k|k-1} = \sum_{i=0}^{2n_x} W_i^{(c)} [\mathcal{X}_{i,k|k-1} - \hat{\mathbf{x}}_{k|k-1}][\mathcal{X}_{i,k|k-1} - \hat{\mathbf{x}}_{k|k-1}]^T + \mathbf{Q}_k$
 - Update:**
 - 15: $\mathcal{Y}_{i,k|k-1} = \mathbf{h}(\mathcal{X}_{i,k|k-1}), i = 0, \dots, 2n_x$
 - 16: $\hat{\mathbf{y}}_{k|k-1} = \sum_{i=0}^{2n_x} W_i^{(m)} \mathcal{Y}_{i,k|k-1}$
 - 17: $\mathbf{P}_{xy,k|k-1} = \sum_{i=0}^{2n_x} W_i^{(c)} [\mathcal{X}_{i,k|k-1} - \hat{\mathbf{x}}_{k|k-1}][\mathcal{Y}_{i,k|k-1} - \hat{\mathbf{y}}_{k|k-1}]^T$
 - 18: $\mathbf{P}_{y,k|k-1} = \sum_{i=0}^{2n_x} W_i^{(c)} [\mathcal{Y}_{i,k|k-1} - \hat{\mathbf{y}}_{k|k-1}][\mathcal{Y}_{i,k|k-1} - \hat{\mathbf{y}}_{k|k-1}]^T$
 - 19: $\mathbf{S}_{k|k-1} = \mathbf{P}_{y,k|k-1} + \mathbf{R}_k$
 - 20: $\mathbf{K} = \mathbf{P}_{xy,k|k-1} \mathbf{S}_{k|k-1}^{-1}$
 - 21: $\hat{\mathbf{x}}_{k|k} = \hat{\mathbf{x}}_{k|k-1} + \mathbf{K}(\mathbf{z}_k - \hat{\mathbf{y}}_{k|k-1})$
 - Recalibrate:**
 - 22: $\mathbf{L}_i = [\sqrt{\mathbf{P}_{k|k-1}}]_i, i = 1, \dots, n_x$
 - 23: $\mathcal{X}_{0,k|k} = \hat{\mathbf{x}}_{k|k}$
 - 24: $\mathcal{X}_{i,k|k} = \hat{\mathbf{x}}_{k|k} + \sqrt{\lambda + n_x} \mathbf{L}_i, i = 1, \dots, n_x$
 - 25: $\mathcal{X}_{i+n_x,k|k} = \hat{\mathbf{x}}_{k|k} - \sqrt{\lambda + n_x} \mathbf{L}_i, i = 1, \dots, n_x$
 - 26: $\mathcal{Y}_{i,k|k} = \mathbf{h}(\mathcal{X}_{i,k|k}), i = 0, \dots, 2n_x$
 - 27: $\hat{\mathbf{y}}_{k|k} = \sum_{i=0}^{2n_x} W_i^{(m)} \mathcal{Y}_{i,k|k}$
 - 28: $\mathbf{P}_{xy,k|k} = \sum_{i=0}^{2n_x} W_i^{(c)} [\mathcal{X}_{i,k|k} - \hat{\mathbf{x}}_{k|k}][\mathcal{Y}_{i,k|k} - \hat{\mathbf{y}}_{k|k}]^T$
 - 29: $\mathbf{P}_{y,k|k} = \sum_{i=0}^{2n_x} W_i^{(c)} [\mathcal{Y}_{i,k|k} - \hat{\mathbf{y}}_{k|k}][\mathcal{Y}_{i,k|k} - \hat{\mathbf{y}}_{k|k}]^T$
 - 30: $\mathbf{S}_{k|k} = \mathbf{P}_{y,k|k} + \mathbf{R}_k$
 - 31: $\mathbf{P}_{k|k} = \mathbf{P}_{k|k-1} + \mathbf{K} \mathbf{S}_{k|k} \mathbf{K}^T - \mathbf{P}_{xy,k|k} \mathbf{K}^T - \mathbf{K} \mathbf{P}_{xy,k|k}^T$
 - Back out:**
 - 32: **if** $\text{tr}(\mathbf{P}_{k|k}) > \text{tr}(\mathbf{P}_{k|k-1})$ **then**
 - 33: $\hat{\mathbf{x}}_{k|k} = \hat{\mathbf{x}}_{k|k-1}$
 - 34: $\mathbf{P}_{k|k} = \mathbf{P}_{k|k-1}$
 - 35: **end if**
 - 36: **end for**
-

Fig. S3. The implementation of the new framework on the unscented Kalman filter. Note that rows 22–35 are replaced by (Eq. 7) in the conventional framework.

Input: Process noise covariance matrix \mathbf{Q}_k , Measurement noise covariance matrix \mathbf{R}_k , states number n_x , state transition function $\mathbf{f}(\mathbf{x}, \mathbf{u})$, measurement function $\mathbf{h}(\mathbf{x})$, system inputs \mathbf{u}_k , measurements \mathbf{z}_k

Initialization:

- 1: $\hat{\mathbf{x}}_{0|0} = \mathbb{E}[\mathbf{x}_0]$
- 2: $\mathbf{P}_{0|0} = \mathbb{E}[(\hat{\mathbf{x}}_{0|0} - \mathbf{x}_0)(\hat{\mathbf{x}}_{0|0} - \mathbf{x}_0)^T]$
- 3: **for** every time step k **do**
- Predict:**
- 4: $\mathbf{L}_i = \lceil \sqrt{\mathbf{P}_{k-1|k-1}} \rceil_i, i = 1, \dots, n_x$
- 5: $\mathcal{X}_{i,k-1} = \hat{\mathbf{x}}_{k-1|k-1} + \sqrt{n_x} \mathbf{L}_i, i = 1, \dots, n_x$
- 6: $\mathcal{X}_{i+n_x,k-1} = \hat{\mathbf{x}}_{k-1|k-1} - \sqrt{n_x} \mathbf{L}_i, i = 1, \dots, n_x$
- 7: $\mathcal{X}_{i,k|k-1}^* = \mathbf{f}(\mathcal{X}_{i,k-1}, \mathbf{u}_{k-1}), i = 1, \dots, 2n_x$
- 8: $\hat{\mathbf{x}}_{k|k-1} = \sum_{i=1}^{2n_x} \frac{1}{2n_x} \mathcal{X}_{i,k|k-1}^*$
- 9: $\mathbf{P}_{k|k-1} = \sum_{i=1}^{2n_x} \frac{1}{2n_x} [\mathcal{X}_{i,k|k-1}^* - \hat{\mathbf{x}}_{k|k-1}][\mathcal{X}_{i,k|k-1}^* - \hat{\mathbf{x}}_{k|k-1}]^T + \mathbf{Q}_k$
- Update:**
- 10: $\mathbf{L}_i = \lceil \sqrt{\mathbf{P}_{k|k-1}} \rceil_i, i = 1, \dots, n_x$
- 11: $\mathcal{X}_{i,k|k-1} = \hat{\mathbf{x}}_{k|k-1} + \sqrt{n_x} \mathbf{L}_i, i = 1, \dots, n_x$
- 12: $\mathcal{X}_{i+n_x,k|k-1} = \hat{\mathbf{x}}_{k|k-1} - \sqrt{n_x} \mathbf{L}_i, i = 1, \dots, n_x$
- 13: $\mathcal{Y}_{i,k|k-1} = \mathbf{h}(\mathcal{X}_{i,k|k-1}), i = 1, \dots, 2n_x$
- 14: $\hat{\mathbf{y}}_{k|k-1} = \sum_{i=1}^{2n_x} \frac{1}{2n_x} \mathcal{Y}_{i,k|k-1}$
- 15: $\mathbf{P}_{xy,k|k-1} = \sum_{i=1}^{2n_x} \frac{1}{2n_x} [\mathcal{X}_{i,k|k-1} - \hat{\mathbf{x}}_{k|k-1}][\mathcal{Y}_{i,k|k-1} - \hat{\mathbf{y}}_{k|k-1}]^T$
- 16: $\mathbf{P}_{y,k|k-1} = \sum_{i=1}^{2n_x} \frac{1}{2n_x} |\mathcal{Y}_{i,k|k-1} - \hat{\mathbf{y}}_{k|k-1}| |\mathcal{Y}_{i,k|k-1} - \hat{\mathbf{y}}_{k|k-1}|^T$
- 17: $\mathbf{S}_{k|k-1} = \mathbf{P}_{y,k|k-1} + \mathbf{R}_k$
- 18: $\mathbf{K} = \mathbf{P}_{xy,k|k-1} \mathbf{S}_{k|k-1}^{-1}$
- 19: $\hat{\mathbf{x}}_{k|k} = \hat{\mathbf{x}}_{k|k-1} + \mathbf{K}(\mathbf{z}_k - \hat{\mathbf{y}}_{k|k-1})$
- Recalibrate:**
- 20: $\mathcal{X}_{i,k|k} = \hat{\mathbf{x}}_{k|k} + \sqrt{n_x} \mathbf{L}_i, i = 1, \dots, n_x$
- 21: $\mathcal{X}_{i+n_x,k|k} = \hat{\mathbf{x}}_{k|k} - \sqrt{n_x} \mathbf{L}_i, i = 1, \dots, n_x$
- 22: $\mathcal{Y}_{i,k|k} = \mathbf{h}(\mathcal{X}_{i,k|k}), i = 1, \dots, 2n_x$
- 23: $\hat{\mathbf{y}}_{k|k} = \sum_{i=1}^{2n_x} \frac{1}{2n_x} \mathcal{Y}_{i,k|k}$
- 24: $\mathbf{P}_{xy,k|k} = \sum_{i=1}^{2n_x} \frac{1}{2n_x} [\mathcal{X}_{i,k|k} - \hat{\mathbf{x}}_{k|k}][\mathcal{Y}_{i,k|k} - \hat{\mathbf{y}}_{k|k}]^T$
- 25: $\mathbf{P}_{y,k|k} = \sum_{i=1}^{2n_x} \frac{1}{2n_x} |\mathcal{Y}_{i,k|k} - \hat{\mathbf{y}}_{k|k}| |\mathcal{Y}_{i,k|k} - \hat{\mathbf{y}}_{k|k}|^T$
- 26: $\mathbf{S}_{k|k} = \mathbf{P}_{y,k|k} + \mathbf{R}_k$
- 27: $\mathbf{P}_{k|k} = \mathbf{P}_{k|k-1} + \mathbf{K} \mathbf{S}_{k|k} \mathbf{K}^T - \mathbf{P}_{xy,k|k} \mathbf{K}^T - \mathbf{K} \mathbf{P}_{xy,k|k}^T$
- Back out:**
- 28: **if** $\text{tr}(\mathbf{P}_{k|k}) > \text{tr}(\mathbf{P}_{k|k-1})$ **then**
- 29: $\hat{\mathbf{x}}_{k|k} = \hat{\mathbf{x}}_{k|k-1}$
- 30: $\mathbf{P}_{k|k} = \mathbf{P}_{k|k-1}$
- 31: **end if**
- 32: **end for**

Fig. S4. The implementation of the new framework on the cubature Kalman filter. Note that rows 20–31 are replaced by (Eq. 7) in the conventional framework.

Input: Process noise covariance matrix \mathbf{Q}_k , Measurement noise covariance matrix \mathbf{R}_k , state transition function $\mathbf{f}(\mathbf{x}, \mathbf{u})$, measurement function $\mathbf{h}(\mathbf{x})$, system inputs \mathbf{u}_k , measurements \mathbf{z}_k

Initialization:

- 1: $\hat{\mathbf{x}}_{0|0} = \mathbb{E}[\mathbf{x}_0]$
- 2: $\mathbf{P}_{0|0} = \mathbb{E}[(\hat{\mathbf{x}}_{0|0} - \mathbf{x}_0)(\hat{\mathbf{x}}_{0|0} - \mathbf{x}_0)^T]$
- 3: **for** every time step k **do**
- Predict:**
- 4: $\mathbf{F}_k = \frac{\partial \mathbf{f}}{\partial \mathbf{x}}|_{\hat{\mathbf{x}}_{k-1|k-1}, \mathbf{u}_{k-1}}$
- 5: $\hat{\mathbf{x}}_{k|k-1} = \mathbf{f}(\hat{\mathbf{x}}_{k-1|k-1}, \mathbf{u}_{k-1})$
- 6: $\mathbf{P}_{k|k-1} = \mathbf{F}_k \mathbf{P}_{k-1|k-1} \mathbf{F}_k^T + \mathbf{Q}_k$
- Update:**
- 7: $\mathbf{x}_0 = \hat{\mathbf{x}}_{k|k-1}$
- 8: **for** $i = 1$ **to** 1000 **do**
- 9: $\mathbf{H}_{k|k-1} = \frac{\partial \mathbf{h}}{\partial \mathbf{x}}|_{\mathbf{x}_{i-1}}$
- 10: $\hat{\mathbf{y}}_{k|k-1} = \mathbf{h}(\mathbf{x}_{i-1}) + \mathbf{H}_{k|k-1}(\mathbf{x}_{i-1} - \hat{\mathbf{x}}_{k|k-1})$
- 11: $\mathbf{P}_{xy,k|k-1} = \mathbf{P}_{k|k-1} \mathbf{H}_{k|k-1}^T$
- 12: $\mathbf{P}_{y,k|k-1} = \mathbf{H}_{k|k-1} \mathbf{P}_{k|k-1} \mathbf{H}_{k|k-1}^T$
- 13: $\mathbf{S}_{k|k-1,i} = \mathbf{P}_{y,k|k-1} + \mathbf{R}_k$
- 14: $\mathbf{K}_i = \mathbf{P}_{xy,k|k-1} \mathbf{S}_{k|k-1,i}^{-1}$
- 15: $\mathbf{x}_i = \hat{\mathbf{x}}_{k|k-1} + \mathbf{K}_i(\mathbf{z}_k - \hat{\mathbf{y}}_{k|k-1})$
- 16: **if** $i > 1$ **and** $\|\mathbf{x}_i - \mathbf{x}_{i-1}\| > \|\mathbf{x}_{i-1} - \mathbf{x}_{i-2}\|$ **then**
- 17: $\mathbf{S}_{k|k-1,i} = \mathbf{S}_{k|k-1,i-1}$
- 18: $\mathbf{K}_i = \mathbf{K}_{i-1}$
- 19: $\mathbf{x}_i = \mathbf{x}_{i-1}$
- 20: **break**
- 21: **end if**
- 22: **if** $\max_j |1 - \mathbf{x}_i(j)/\mathbf{x}_{i-1}(j)| < 0.001$ **then**
- 23: **break**
- 24: **end if**
- 25: **end for**
- 26: $\mathbf{S}_{k|k-1} = \mathbf{S}_{k|k-1,i}$
- 27: $\mathbf{K} = \mathbf{K}_i$
- 28: $\hat{\mathbf{x}}_{k|k} = \mathbf{x}_i$
- Recalibrate:**
- 29: $\mathbf{H}_{k|k} = \frac{\partial \mathbf{h}}{\partial \mathbf{x}}|_{\hat{\mathbf{x}}_{k|k}}$
- 30: $\mathbf{P}_{xy,k|k} = \mathbf{P}_{k|k-1} \mathbf{H}_{k|k}^T$
- 31: $\mathbf{P}_{y,k|k} = \mathbf{H}_{k|k} \mathbf{P}_{k|k-1} \mathbf{H}_{k|k}^T$
- 32: $\mathbf{S}_{k|k} = \mathbf{P}_{y,k|k} + \mathbf{R}_k$
- 33: $\mathbf{P}_{k|k} = \mathbf{P}_{k|k-1} + \mathbf{K} \mathbf{S}_{k|k} \mathbf{K}^T - \mathbf{P}_{xy,k|k} \mathbf{K}^T - \mathbf{K} \mathbf{P}_{xy,k|k}^T$
- Back out:**
- 34: **if** $\text{tr}(\mathbf{P}_{k|k}) > \text{tr}(\mathbf{P}_{k|k-1})$ **then**
- 35: $\hat{\mathbf{x}}_{k|k} = \hat{\mathbf{x}}_{k|k-1}$
- 36: $\mathbf{P}_{k|k} = \mathbf{P}_{k|k-1}$
- 37: **end if**
- 38: **end for**

Fig. S5. The iterated extended Kalman filter algorithm used in this paper. Note that rows 16–21 are added to prevent the state estimations from diverging. In the algorithm, when the sign of divergence is detected (row 16), the newest updates of the states, Kalman gain, and measurement residual covariance matrix are withdrawn (rows 17–19). If such a withdrawal is not made, we found in the simulation that the estimation accuracy can be much lower. This characteristic also suggests that the algorithm is not very robust and stable.

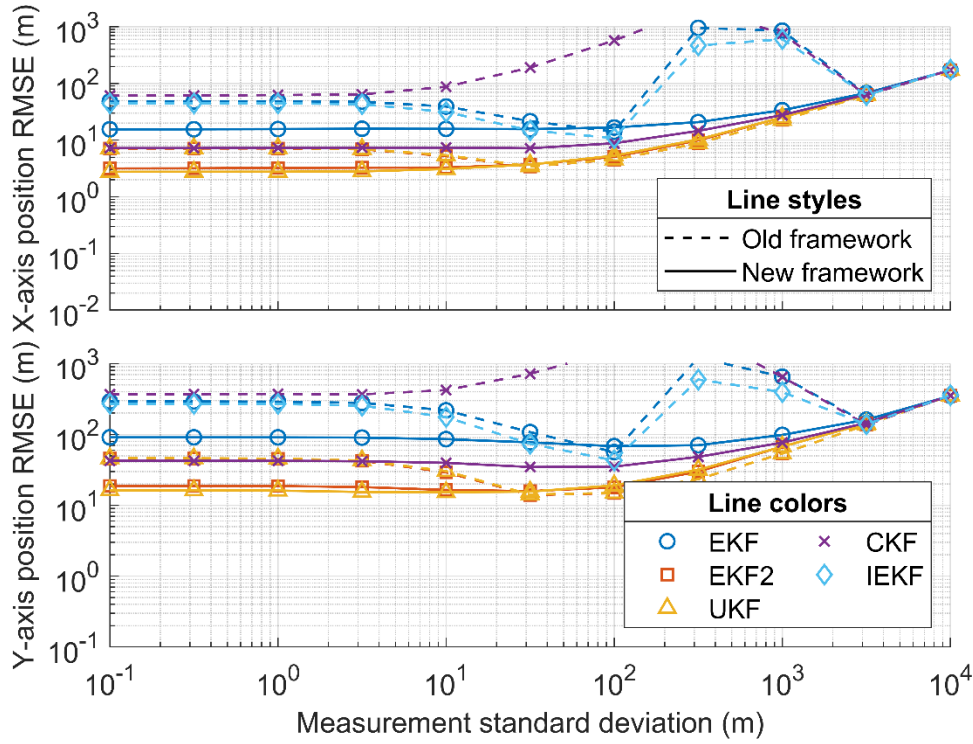


Fig. S6. The root mean squared error of the state estimations under different measurement noise setups (terrain-referenced navigation). Different types of nonlinear Kalman filters are represented by different colors and markers, while the old and new frameworks are represented by dotted lines and solid lines, respectively. The root mean squared error is calculated from the estimation errors in 10,000 simulations. The estimation error is calculated as the difference between the estimated state and the true state at the end of the final iteration of each simulation. The measurement is the terrain's elevation at the present location.

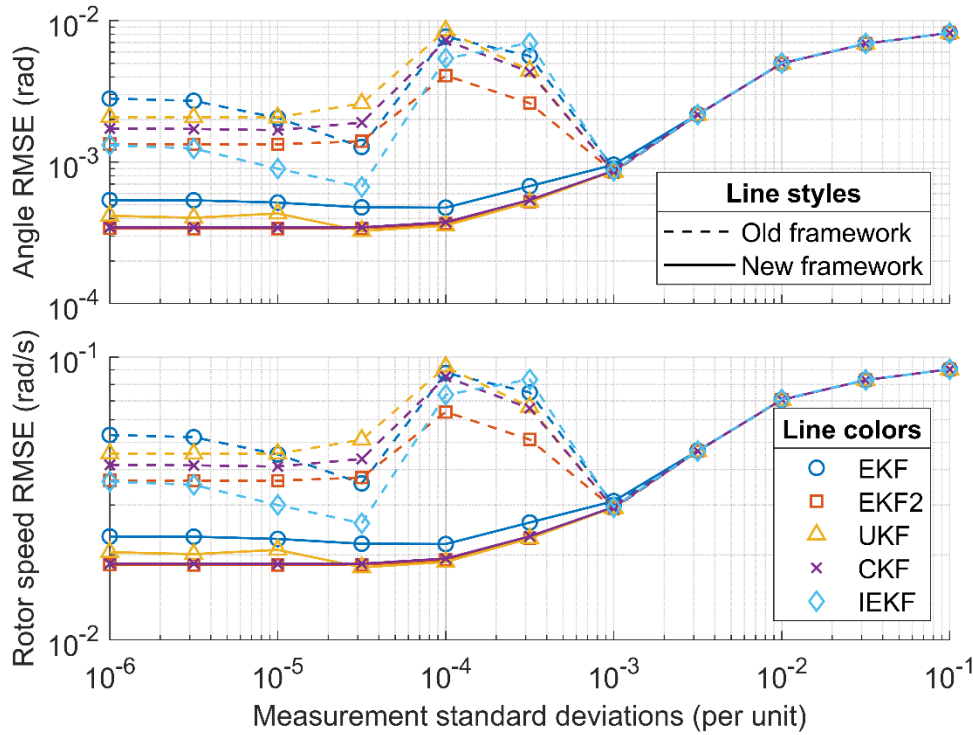


Fig. S7. The root mean squared error of the state estimations under different measurement noise setups (synchronous generator state estimation). Different types of nonlinear Kalman filters are represented by different colors and markers, while the old and new frameworks are represented by dotted lines and solid lines, respectively. The root mean squared error is calculated from the estimation errors in 10,000 simulations. The estimation error is calculated as the difference between the estimated state and the true state at the end of the final iteration of each simulation. The measurement is the electrical output power in per-unit value.

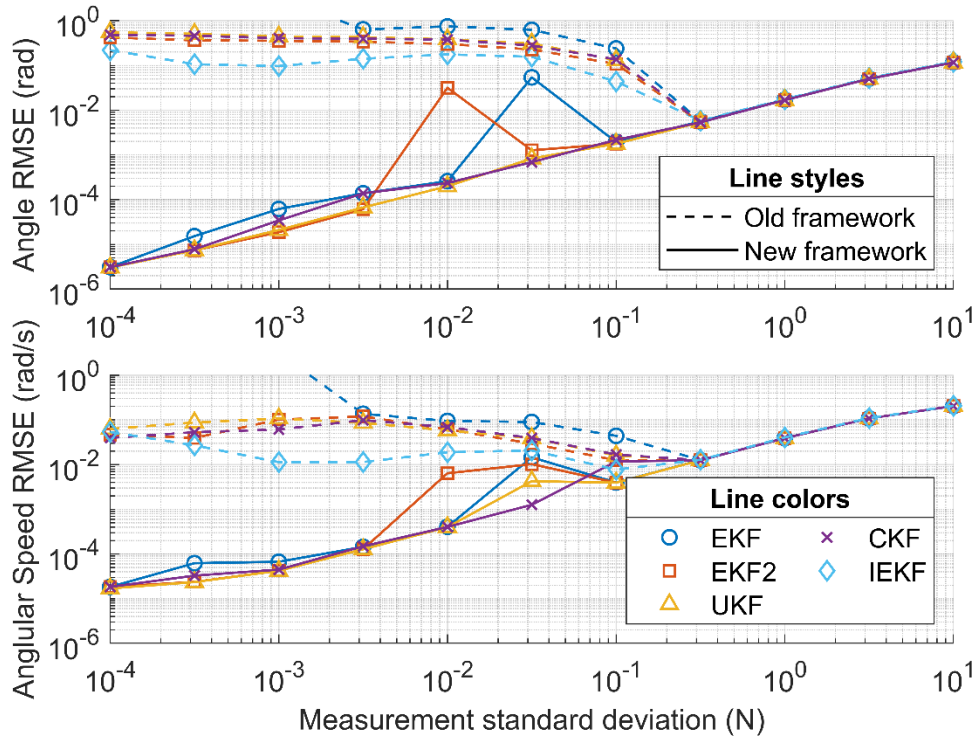


Fig. S8. The root mean squared error of the state estimations under different measurement noise setups (pendulum state estimation). Different types of nonlinear Kalman filters are represented by different colors and markers, while the old and new frameworks are represented by dotted lines and solid lines, respectively. The root mean squared error is calculated from the estimation errors in 10,000 simulations. The estimation error is calculated as the difference between the estimated state and the true state at the end of the final iteration of each simulation. The measurement is the horizontal component of tension in the rope.

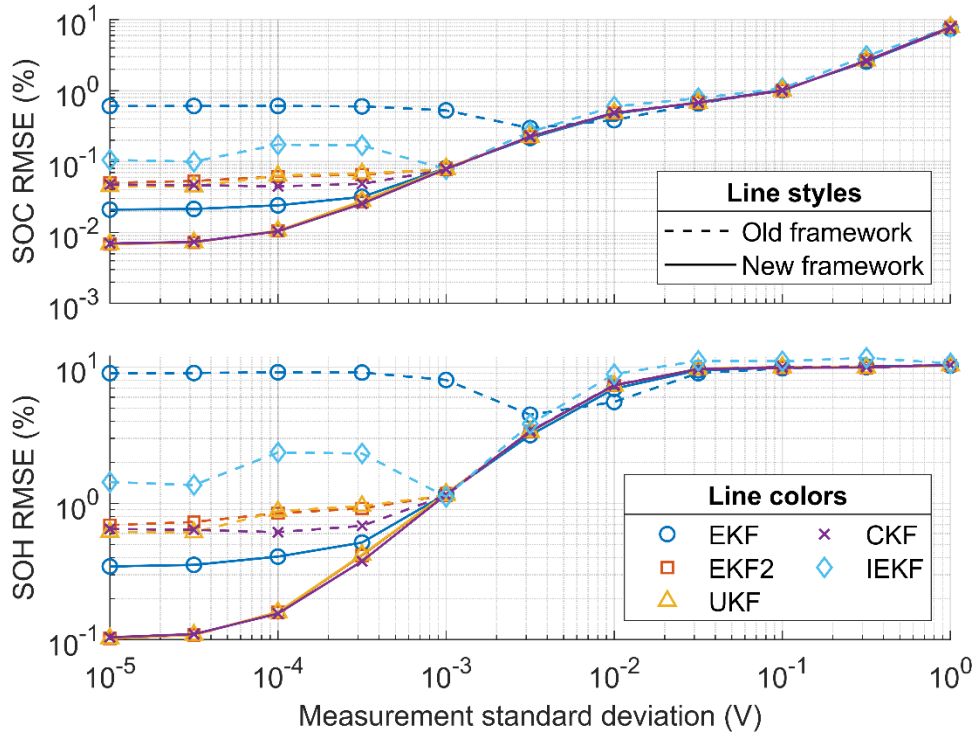


Fig. S9. The root mean squared error of the state estimations under different measurement noise setups (battery state estimation). Different types of nonlinear Kalman filters are represented by different colors and markers, while the old and new frameworks are represented by dotted lines and solid lines, respectively. The x-axis represents the standard deviations of the measurements from the voltmeter. The root mean squared error is calculated from the estimation errors in 10,000 simulations. The estimation error is calculated as the difference between the estimated state and the true state at the end of the final iteration

of each simulation. The measurement is the battery's terminal voltage. SOC, the state of charge, is defined as the ratio of the present capacity to its maximum value. SOH, the state of health, is the ratio of the present maximum capacity to its initial value. SOC characterizes the battery's energy level, and SOH characterizes the battery's aging level.

References and Notes

1. D.-J. Jwo, T.-S. Cho, Critical remarks on the linearised and extended Kalman filters with geodetic navigation examples. *Measurement* **43**, 1077–1089 (2010).
2. T. T. Phuong, K. Ohishi, C. Mitsantisuk, Y. Yokokura, K. Ohnishi, R. Oboe, A. Sabanovic, Disturbance Observer and Kalman Filter Based Motion Control Realization. *IEEJ Journal of Industry Applications* **7**, 1–14 (2018).
3. E. N. Brown, C. H. Schmid, “[9] Application of the Kalman filter to computational problems in statistics” in *Methods in Enzymology* (Academic Press, 1994; <https://www.sciencedirect.com/science/article/pii/S0076687994400482>)vol. 240 of *Part B: Numerical Computer Methods*, pp. 171–181.
4. M. Roth, G. Hendeby, C. Fritsche, F. Gustafsson, The Ensemble Kalman filter: a signal processing perspective. *EURASIP Journal on Advances in Signal Processing* **2017**, 56 (2017).
5. K. P. B. Chandra, D.-W. Gu, *Nonlinear Filtering: Methods and Applications* (Springer, New York, NY, 1st ed. 2019 edition., 2018).
6. T. A. S. Corporation, *Applied Optimal Estimation* (MIT Press, 1974).
7. S. J. Julier, J. K. Uhlmann, “New extension of the Kalman filter to nonlinear systems” in *Signal Processing, Sensor Fusion, and Target Recognition VI* (SPIE, 1997; <https://www-spiedigitallibrary-org.libproxy.berkeley.edu/conference-proceedings-of-spie/3068/0000/New-extension-of-the-Kalman-filter-to-nonlinear-systems/10.1117/12.280797.full>)vol. 3068, pp. 182–193.
8. E. A. Wan, R. Van Der Merwe, “The unscented Kalman filter for nonlinear estimation” in *Proceedings of the IEEE 2000 Adaptive Systems for Signal Processing, Communications, and Control Symposium (Cat. No.00EX373)* (2000; <https://ieeexplore-ieee-org.libproxy.berkeley.edu/abstract/document/882463>), pp. 153–158.
9. I. Arasaratnam, S. Haykin, Cubature Kalman Filters. *IEEE Transactions on Automatic Control* **54**, 1254–1269 (2009).
10. I. Arasaratnam, S. Haykin, R. J. Elliott, Discrete-Time Nonlinear Filtering Algorithms Using Gauss–Hermite Quadrature. *Proceedings of the IEEE* **95**, 953–977 (2007).
11. I. Arasaratnam, S. Haykin, Square-Root Quadrature Kalman Filtering. *IEEE Transactions on Signal Processing* **56**, 2589–2593 (2008).
12. F. Gustafsson, G. Hendeby, Some Relations Between Extended and Unscented Kalman Filters. *IEEE Transactions on Signal Processing* **60**, 545–555 (2012).
13. B. Bell, F. Cathey, The Iterated Kalman Filter Update as a Gauss-Newton Method. *IEEE Trans. Autom. Control* **38**, 294–297 (1993).

14. R. Zhan, J. Wan, Iterated Unscented Kalman Filter for Passive Target Tracking. *IEEE Transactions on Aerospace and Electronic Systems* **43**, 1155–1163 (2007).
15. J. Mu, Y. Cai, “Iterated cubature Kalman filter and its application” in *2011 IEEE International Conference on Cyber Technology in Automation, Control, and Intelligent Systems* (2011; https://ieeexplore-ieee-org.libproxy.berkeley.edu/abstract/document/6011759?casa_token=2qVviKGBkikAAAAA:r pFDfi7v69MOKBvEdyYsi8uMFSXrJi9q18BK2bHOSlRs6SZErHicwyi9iGf1ZTrxTEIFRFtRLvA), pp. 33–37.
16. J. Havlik, O. Straka, “Performance evaluation of iterated extended Kalman filter with variable step-length” in *12TH EUROPEAN WORKSHOP ON ADVANCED CONTROL AND DIAGNOSIS (ACD 2015)* (IoP Publishing Ltd, Bristol, 2015; <https://iopscience-iop-org.libproxy.berkeley.edu/article/10.1088/1742-6596/659/1/012022>) vol. 659 of *Journal of Physics Conference Series*, p. 012022.
17. L. Chang, B. Hu, G. Chang, A. Li, Marginalised iterated unscented Kalman filter. *IET Control Theory & Applications* **6**, 847–854 (2012).
18. G. Chang, T. Xu, Q. Wang, Alternative framework for the iterated unscented Kalman filter. *IET Signal Processing* **11**, 258–264 (2017).
19. S. Sarkka, On Unscented Kalman Filtering for State Estimation of Continuous-Time Nonlinear Systems. *IEEE Transactions on Automatic Control* **52**, 1631–1641 (2007).
20. Y. Kim, H. Bang, Y. Kim, H. Bang, “Introduction to Kalman Filter and Its Applications” in *Introduction and Implementations of the Kalman Filter* (IntechOpen, 2018; <https://www.intechopen.com/chapters/63164>).
21. E. Ghahremani, I. Kamwa, Online State Estimation of a Synchronous Generator Using Unscented Kalman Filter From Phasor Measurements Units. *IEEE Transactions on Energy Conversion* **26**, 1099–1108 (2011).
22. S. Jiang, J. Shi, M. Borah, S. Moura, “Weaknesses and Improvements of the Extended Kalman Filter for Battery State-of-Charge and State-of-Health Estimation” in *2024 American Control Conference (ACC)* (2024; <https://ieeexplore.ieee.org/abstract/document/10644628>), pp. 1441–1448.

Acknowledgments:

Funding: This material is based upon work supported, in part, by the National Science Foundation under Grant No. 1847177.

Competing interests: Authors declare that they have no competing interests.

Data and materials availability: All the codes related to this paper can be found online at <https://github.com/Shida-Jiang/A-new-framework-for-nonlinear-Kalman-filters>. All the figures and tables in this paper can be reproduced simply by running all the codes. No dataset is used in this study.